Laser Welding of Ruptured Intestinal Tissue Using Plasmonic Polypeptide Nanocomposite Solders

Huang-Chiao Huang,[†] Candace Rae Walker,[‡] Alisha Nanda,[†] and Kaushal Rege[†,‡,*]

[†]Chemical Engineering and [‡]Biomedical Engineering Arizona State University, Tempe, Arizona 85287-6106, United States

ABSTRACT Approximately 1.5 million people suffer from colorectal cancer and inflammatory bowel disease in the United States. Occurrence of leakage following standard surgical anastomosis in intestinal and colorectal surgery is common and can cause infection leading to life-threatening consequences. In this report, we demonstrate that plasmonic nanocomposites, generated from elastin-like polypeptides (ELPs) cross-linked with gold nanorods, can be used to weld ruptured intestinal tissue upon exposure to near-infrared (NIR) laser irradiation. Mechanical properties of these nanocomposites can be modulated based on the concentration of gold nanorods embedded within the ELP matrix. We employed photostable, NIR-absorbing cellularized and noncellularized GNR—ELP nanocomposites for *ex vivo* laser welding of ruptured porcine small intestines. Laser welding using the nanocomposites significantly enhanced the tensile strength, leakage pressure, and bursting pressure of ruptured intestinal tissue. This, in turn, provided a liquid-tight seal against leakage of luminal liquid from the intestine and resulting bacterial infection. This study demonstrates the utility of laser tissue welding using plasmonic polypeptide nanocomposites and indicates the translational potential of these materials in intestinal and colorectal repair.

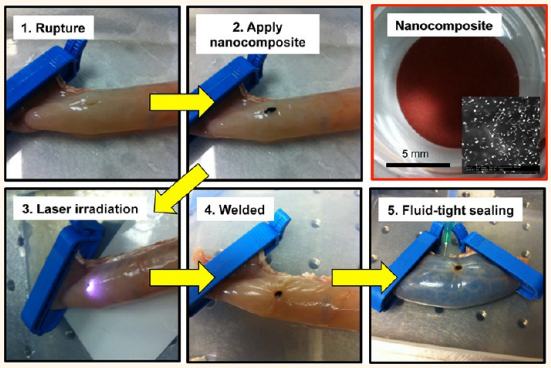

KEYWORDS: gold nanorods · elastin-like polypeptide · plasmonic biomaterials · laser tissue welding

Colorectal diseases that may require surgical intervention include colorectal cancer and inflammatory bowel disease (IBD) among others. Approximately 143 000 and 1.4 million people suffer from colorectal cancer and IBD, respectively, in the United States (National Cancer Institute and Centers for Disease Control and Prevention). Colorectal resection, or colectomy, involves the removal of bowel tissue affected by disease and the rejoining (anastomosis) of healthy ends by surgical suturing and stapling. Incidence of leakage following standard surgical anastomosis is reported to occur in 4—17% of cases with colorectal surgery and can cause serious bacterial infection, leading to life-threatening consequences.[1—6]

Laser tissue welding (LTW) is a "stitch-free" surgical method for the anastomosis of ruptured tissues including articular cartilage,[7] blood vessels,[8] cornea,[9] liver,[10] urinary tract,[11] nerve,[12] and skin.[13,14] The mechanism for LTW involves the tissue absorption of laser light, which is converted to heat energy, resulting in deformation of tissue proteins and eventually their fusion.[12,15] Interdigitation of the photothermally altered tissue proteins (*e.g.*, type I collagen fibrils) *via* covalent (*e.g.*, disulfide) and electrostatic interactions[9,16,17] is considered to be the basic mechanism for tissue welding following laser treatment.

Laser tissue welding possesses several advantages over conventional suturing and stapling procedures for repair and healing of ruptured tissues. These include short operation times, immediate fluid-tight sealing, reduced foreign body reactions (*e.g.*, inflammatory response), scar reduction, and accelerated healing.[18—21] Moreover, laser tissue welding is particularly applicable in regions where suturing and stapling may not be feasible. Major concerns associated with traditional LTW carried out with laser irradiation alone include insufficient anastomoses strength, low depths of light penetration, and peripheral tissue thermal damage. These limitations can be potentially addressed by the introduction of

* Address correspondence to kaushal.rege@asu.edu.

Received for review July 17, 2012 and accepted March 26, 2013.

Published online March 26, 2013
10.1021/nn303202k

exogenous protein-based solders in concert with near-infrared (NIR) light absorbing chromophores.[22,23] Upon laser irradiation of the chromophores, the protein solders denature and can be incorporated into the weld site, leading to improved tensile strength of the closure, minimized peripheral tissue destruction, and reduction in foreign body responses. Use of NIR irradiation enables deeper tissue penetration.

Here, we show *ex vivo* laser welding of ruptured small intestinal tissue using novel gold nanorod–elastin-like polypeptide (GNR–C_{12}ELP) plasmonic nanocomposites.[24] The current work possesses several advantages for laser-based repair of tissues, particularly compared to organic chromophores: (1) gold nanorods possess higher photochemical stability and minimum diffusivity compared to organic chromophores;[25] (2) gold nanorods, which possess high near-infrared absorption cross-section, can convert light into heat more efficiently compared to conventional dyes (*e.g.*, indocyanine green).[26,27] This, in turn, can potentially reduce thermal damage of the peripheral tissue. (3) Engineered elastin-like polypeptides (ELPs) are biocompatible, demonstrate low immunogenicities,[28,29] and have been employed for several biomedical applications,[30,31] including wound healing.[29] Plasmonic nanocomposites, in which ELPs are cross-linked using gold nanorods, can provide improved dynamic shear stiffness as well as stretch/recoil properties that mimic the wound-healing environment during the proliferation (granulation) stage. The elasticity of the GNR–C_{12}ELP nanocomposite can allow for recovery of intestinal and colorectal function. In this report, we therefore characterized the mechanical properties of GNR–C_{12}ELP plasmonic nanocomposites and evaluated the tensile strength, leaking and bursting pressures, and bacterial leakage following *ex vivo* laser tissue welding of porcine intestinal tissue with and without the plasmonic nano composite. Our results demonstrate that GNR–C_{12}ELP plasmonic nanocomposites may be attractive materials for surgical repair and regeneration applications.

RESULTS AND DISCUSSION

Self-assembly of thermally responsive C_{12}ELPs (ELPs containing 12 cysteines in the polypeptide repeat sequence; transition temperature T_t = 30.4 °C) on GNRs (λ_{max} = 780 nm) was facilitated by gold–thiol bonds, resulting in the formation of well-dispersed nanoassemblies at 4 °C. Incubation of the nanoassemblies at 37 °C (>T_t of C_{12}ELP) for 6 h led to temperature-triggered, entropy-dominated phase transition of C_{12}ELP,[32] which, in concert with GNR–thiol and intra- and intermolecular cysteine–cysteine cross-linking, resulted in the formation of maroon-colored plasmonic nanocomposites as precipitates (Figure 1A).[24] Typically, the solid-phase GNR–C_{12}ELP nanocomposites were 10 mm in diameter, 2.2 ± 0.2 mg in weight, and 247 ± 65 μm thick, as determined using a digital caliper

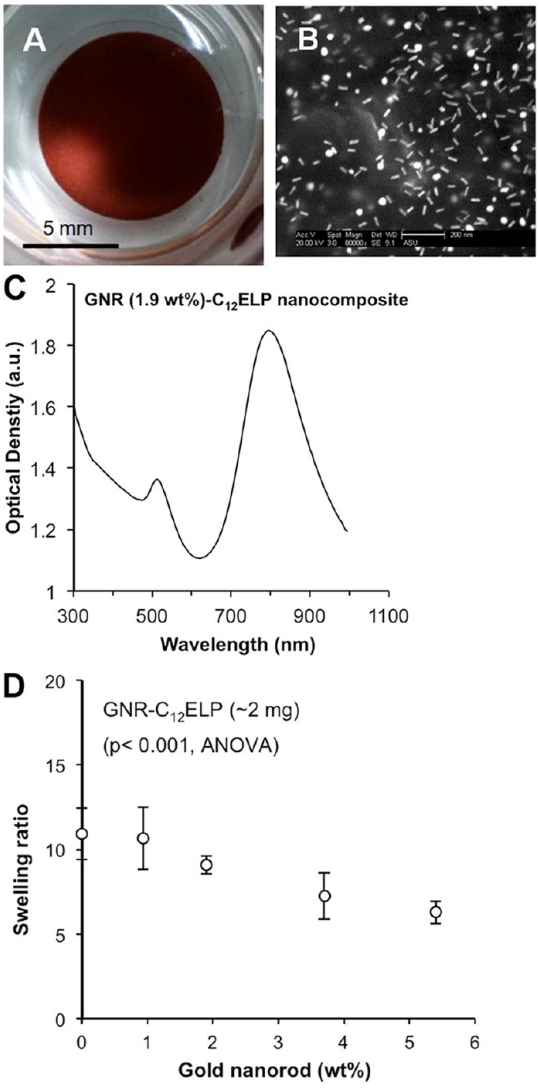

Figure 1. (A) Digital image of GNR (5.4 wt %)–C_{12}ELP nanocomposite. (B) Environmental field-emission scanning electron microscopy (FE-SEM) images of GNR–C_{12}ELP nanocomposites. Microscopy (PHILIPS FEI XL-30 SEM), operated at an accelerating voltage of 25 kV, indicated uniform distribution of gold nanorods throughout the polypeptide matrix in the nanocomposite. Gold nanorods are ~15 nm in diameter, ~50 nm in length (scale bar: 200 nm). (C) Absorbance spectra of GNR (5.4 wt %)–C_{12}ELP nanocomposite. (D) Swelling experiments reveal a statistically significant (p < 0.001) reduction in swelling capacity with an increase in GNR weight percentage (wt %). Each data point represents the mean of at least three measurements. Statistical significance (p-value <0.05) was determined using one-way ANOVA (Minitab).

and light microscopy. Gold nanorods were uniformly distributed throughout the C_{12}ELP matrix, as visualized by field emission scanning electron microscopy (FE-SEM) (Figure 1B). The absorbance spectra of nanocomposites (Figure 1C) demonstrated both transverse (λ_{max} = 520 nm) and red-shifted longitudinal bands (λ_{max} = ~800 nm). These are characteristic of the embedded gold nanorods and reflect the plasmonic properties of these nanocomposites. The red shift in the longitudinal peak is likely due to a change in dielectric constant of the

local environment around GNRs due to the presence of the C_{12}ELP polypeptide.[24]

Engineered ELPs are promising materials in several biomedical applications, but their low dynamic shear stiffness can be limiting for regenerative medicine applications that require load-bearing properties.[33] By incorporating GNRs within the ELP matrix, we demonstrated the ability to modulate swelling and absolute shear modulus of these plasmonic nanocomposites. A statistically significant ($p < 0.001$) reduction in the swelling ratio from 11 to 6 was observed when the weight percentage of GNRs increases from 0% to 5.4% (Figure 1D). Increase in GNR content facilitates cross-linking, which results in the formation of a more rigid network with reduced swelling properties.

Rheological properties of C_{12}ELP coacervates formed in the absence of GNRs and GNR−C_{12}ELP nanocomposites (GNR wt %: 0.47, 0.9, 1.9, and 3.7) were measured under frequency sweep (Figure 2A, B) and temperature sweep (Figure 2C, D) conditions. C_{12}ELP coacervates possess an absolute shear modulus ($|G^*|$; also known as dynamic shear stiffness) of approximately 0.56 ± 0.1 kPa (Figure 2A). Previous reports indicate that $|G^*|$ of non-cross-linked ELP was approximately 0.08 kPa,[34] while that of chemically cross-linked ELPs ranged from 0.26 to 3 kPa.[33,35] The absolute shear modulus of C_{12}ELP coacervates is similar to that of chemically cross-linked ELPs, presumably due to the presence of intra- and intermolecular cysteine−cysteine cross-linking.[24] The absolute shear modulus of C_{12}ELP coacervates was further enhanced with the introduction of GNRs. The $|G^*|$ of GNR−C_{12}ELP nanocomposite increased from ~2 kPa to ~8 kPa as GNR weight percentage increased from 0.47 wt % to 3.7 wt %. The increase in material stiffness (or $|G^*|$) is due to the presence of gold nanorods in the nanocomposite.

All nanocomposites demonstrated predominantly elastic behavior, as reflected by the values of loss angles (δ), which were less than 10 degrees in the cases investigated; the mean value of tan δ of the nanocomposites was independent of GNR concentration (Figure 2B). Increase in temperature from 25 °C to 45 °C did not influence the absolute shear moduli of nanocomposites (Figure 2C and D). The loss angle of the nanocomposites was also independent of temperature, reflecting the intrinsically stable elastic behavior of nanocomposites under normal and moderately hyperthermic physiological conditions. This is particularly significant for repair of intestinal and colorectal tissues, which require material elasticity

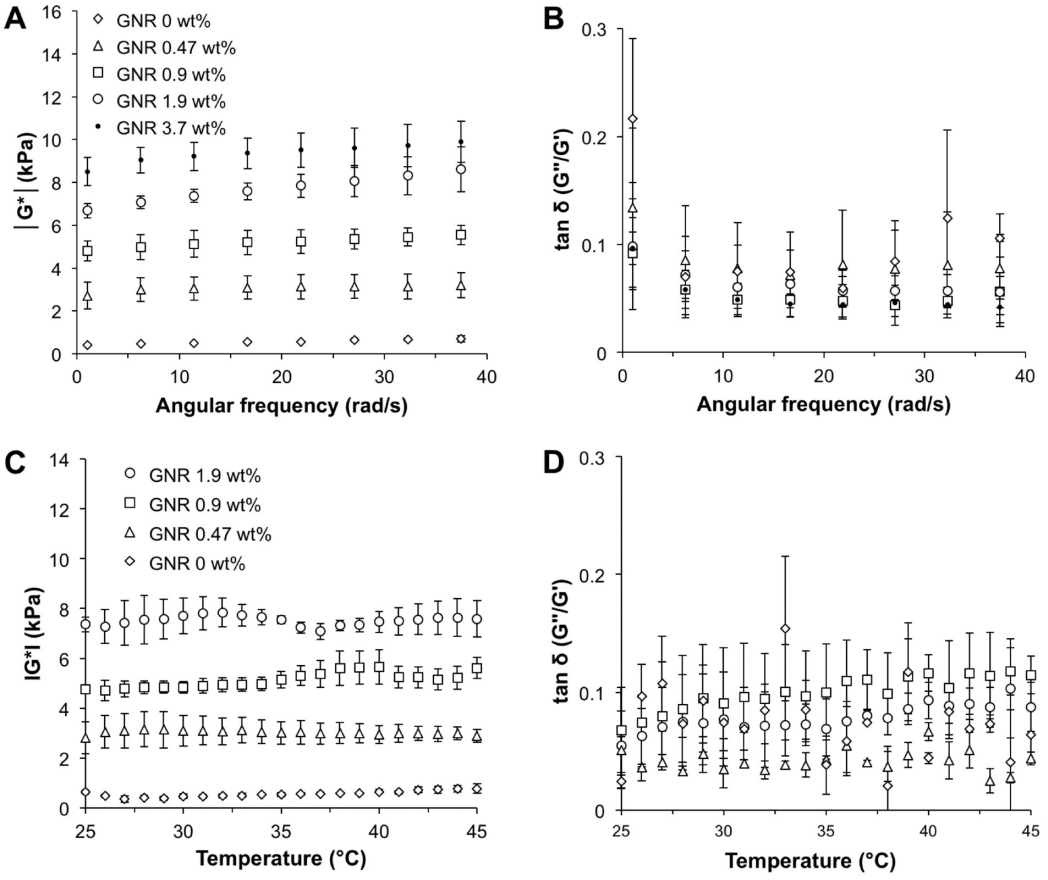

Figure 2. Rheological behavior of GNR−C_{12}ELP nanocomposites. (A and B) Frequency sweep. (C and D) Temperature sweep. The absolute shear modulus ($|G^*|$) remained stable with ascending frequency, but increases with gold nanorod content. All nanocomposite samples showed a predominantly elastic behavior with small loss angle (tan δ) values.

for their function. Thus, cross-linking cysteine-containing ELPs using gold nanorods can significantly improve the ELP dynamic shear stiffness in a tunable manner and result in elastic nanocomposites. In addition, the ELP molecules provide a confinement barrier around GNRs, which not only can maintain GNR stability in physiological environments but can also facilitate better control of the local nanorod density, thereby resulting in a reproducible photothermal response.

Biocompatible ELP-based hydrogels, aggregates, and micelles can support cell proliferation and/or differentiation for vascular graft, cartilage, ocular, and liver tissue engineering.[33,36−40] Given that cellularized scaffolds may play a role in accelerating the repair and regeneration of tissues, we wanted to determine whether GNR−C_{12}ELP nanocomposites could support cell culture and proliferation. We demonstrated that murine fibroblasts could adhere as well as proliferate when cultured on top of nanocomposites (Figures S1, S2, and S3, Supporting Information). In Figure S1A, the number of cells attached on top of GNR−C_{12}ELP nanocomposites was approximately 60% of that observed in the case of the tissue culture plastic control, 24 h after cell seeding (Figure S1, dotted line). Increasing the GNR weight percentage in the nanocomposites from 1.9 to 5.4 resulted in an approximately 25% decrease in cell adhesion density ($p < 0.001$). Reduced cell adhesion and proliferation on the nanocomposite surface may be in part due to the nature of the surface chemistry of the nanocomposites. We also investigated polyethylene glycol (PEG)-modified GNRs for cross-linking C_{12}ELPs. This resulted in the formation of PEG−GNR−C_{12}ELP nanocomposites, with various PEG weight percentages (4.7−19.7 wt %) and a fixed GNR concentration (1.9 wt %). Significantly higher ($p < 0.001$) cell adhesion density was observed on PEG−GNR−C_{12}ELP nanocomposites (~110 cells/mm^2), compared to GNR−C_{12}ELP nanocomposites (~75 cells/mm^2), after 24 h of cell seeding (Figure S1B). Fibroblast cell proliferation on PEG−GNR−C_{12}ELP nanocomposites was up to 30% higher than in the case of unmodified GNR−C_{12}ELP nanocomposites. Although fibroblasts adhered and proliferated on both PEG-modified and unmodified GNR-based nanocomposites, their proliferation was less than that observed on tissue culture plastic control (Figure S2). However, the viability of cells adhered on all nanocomposites was greater than 90−95% in most cases (Figure S3). Taken together, the nanocomposites were able to support fibroblast growth and proliferation with negligible toxicity, indicating that both the cellularization potential and the plasmonic properties of these nanocomposites can be employed in tissue repair and regeneration applications.

We next investigated both cellularized (PEG−GNR−C_{12}ELP) nanocomposites and noncellularized (GNR−C_{12}ELP) nanocomposites as solders for laser-based welding of porcine small intestines *ex vivo*. We chose PEG−GNR−C_{12}ELP for the cellularization studies since they showed modestly higher cell proliferation compared to GNR−C_{12}ELP nanocomposites. The injury model employed in this study is representative of bowel tissue after conventional anastamoses with leakage. Following an incision injury to the intestine, the plasmonic nanocomposite (1 mm diameter and ~2 mg) was applied to the site of the injury, followed by laser-based photothermal treatment. The tensile strength of the rectangular tissue section was determined in order to evaluate the mechanical integrity of different treatments (Figure 3A). As expected, ruptured and intact small intestine sections possess the lowest (0.11 ± 0.01 MPa) and highest (0.45 ± 0.02 MPa) ultimate tensile strengths, respectively (Figure 3B). In the absence of the plasmonic nanocomposites, laser irradiation alone (20 W/cm^2, 1 mm/s, and 3 min) across the incision did not enhance the tensile strength of the ruptured intestine. In the absence of laser irradiation, nanocomposites alone demonstrated negligible adhesion and enhanced the tensile strength of the ruptured tissue by a modest amount (~0.03 MPa; $p = 0.052$, $n = 11$).

NIR laser irradiation (20 W/cm^2; constant speed of 1 mm/s) of GNR−C_{12}ELP nanocomposites containing 1.9, 5.4, and 8.7 wt % GNRs resulted in bulk temperatures of 46 ± 1.1, 61 ± 1.5, and 64 ± 0.9 °C, respectively ($n = 9$), due to the photothermal properties of these plasmonic biomaterials. It is likely that the temperature at the site of the weld may be much higher than the bulk temperature. Irradiating ruptured intestines using nanocomposites containing 1.9 and 5.4 wt % GNR with an NIR laser for only one minute resulted in an increase in the tissue ultimate tensile strength up to 0.17 ± 0.01 and 0.22 ± 0.01 MPa, respectively. The higher recovery in the case of a GNR concentration of 5.4 wt % may be due to the higher welding temperature (61 ± 1.5 °C) attained in this case. It is typically necessary to heat tissues above 60 °C in order to induce coagulation of proteins for obtaining robust welds.[18,41] Increasing the laser irradiation time from 1 min to 7 min and increasing the GNR content in nanocomposites from 5.4 wt % to 8.7 wt % did not enhance the tensile strength of the welded tissue further. Standard suturing techniques allow for up to 60% recovery of the mechanical strength of ruptured bowel intestinal tissue by 3 to 4 days.[42,43] We demonstrated that laser treatment in combination with nanocomposites could enhance the tensile strength of ruptured intestinal sections up to approximately 47% of the original intact form.

We also used cellularized (fibroblast-containing) PEG−GNR−C_{12}ELP nanocomposites for welding the ruptured intestine (Figure 3C); fibroblasts were cultured on top of the nanocomposites (PEG 4.7 wt % and GNR 1.9 wt %) for 1, 4, and 7 days before laser tissue welding. In all cases, welding strengths were similar to those observed with acellular nanocomposites, indicating that materials cellularized with judicious choice of cells can further participate in repair

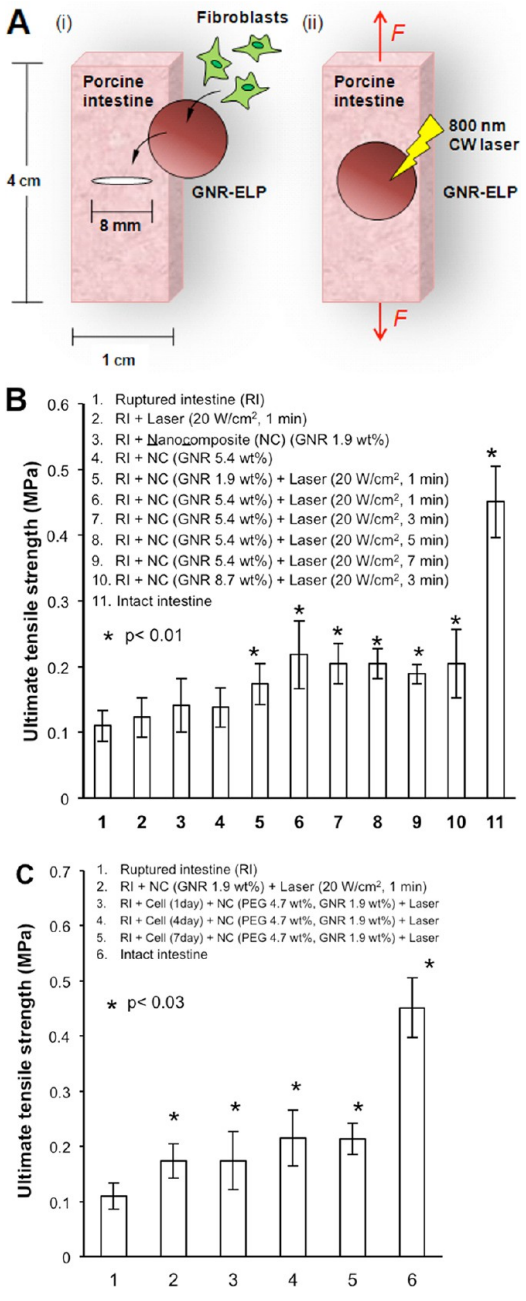

Figure 3. (A) (i) Schematic depicting the experimental setup for laser tissue welding. (ii) NIR laser light was irradiated across the nanocomposite (with or without cells) placed on top of the incision. The welded tissue was then subjected to tensile strength measurement (F: force). (B) Ultimate tensile strength of tissues before and after laser tissue welding using (GNR–C_{12}ELP) nanocomposites. (C) Ultimate tensile strength of tissues before and after laser tissue welding using cellularized (PEG–GNR–C_{12}ELP) nanocomposites. Fibroblasts were cultured on top of nanocomposites for 1, 4, and 7 days.

and regeneration of welded tissues. The lack of tensile strength enhancement of fibroblast-cultured nanocomposites may be partially due to insufficient stroma production likely as a result of the relatively low density of cells cultured on the nanocomposites. It has been reported that stroma production by fibroblasts occurs at a significantly higher rate once cultured cells reach confluence (or at the stationary phase) than in the exponential growth phase of culture.[44] Other studies demonstrated that changes in the microenvironment (*e.g.*, cell culture substrate material) can significantly affect, and likely decrease, stroma production by NIH 3T3 cells.[45,46] It is likely that the relatively low density of fibroblasts, as well as the microenvironment of nanocomposites, resulted in insufficient production of stroma, which in turn was responsible for the lack of enhancement in tensile strength upon cellularization with NIH 3T3 fibroblasts.

A critical aspect of sealing intestinal and colorectal tissues involves prevention of leakage of luminal fluid after anastomosis. Exposure of surrounding tissues to this bacteria-rich fluid can result in sustained inflammation, shock, and mortality.[47−49] To ensure that nanocomposite-assisted laser tissue welding results in fluid-tight sealing, we investigated (i) the leakage and bursting pressure (defined in the Experimental Section) and (ii) bacterial leakage following welding. Nanocomposites (~2 mg), at a fixed GNR concentration of 5.4 wt %, were first applied to the 5 mm cut (Figure 4A, B), followed by laser irradiation (Figure 4C, D), leading to a temperature increase of up to 61 ± 1.5 °C. The leakage and bursting pressures were measured immediately after anastomosis (Figure 4E) using a homemade device and reported in pounds per square inch (psi) (Figure 4F). As expected, the ruptured and intact intestine demonstrated the lowest and highest leakage/bursting pressures, respectively. In the case of ruptured intestines, bursting was observed immediately and was followed by leakage. Both the leakage and bursting pressures were approximately 0.2 psi. In the case of intact intestines, the first evidence of leakage was observed at the needle-piercing site at a pressure of 7.2 psi, while bursting was observed along the tissue when the pressure reached 12 psi. Ruptured intestines treated with laser alone (without nanocomposite) and nanocomposite alone (without laser treatment) demonstrated negligible leakage/bursting pressures (<1 psi), indicating that these treatments had a minimal effect on repair. Laser irradiation of the nanocomposite at the incision site increased both the tissue leakage and bursting pressures. Increasing the laser irradiation time from 1 min to 7 min resulted in an increase in both leakage and bursting pressures to 5 ± 1.3 and 5.8 ± 0.5 psi, respectively. In these cases, bursting immediately followed leakage, as reflected by similar values for leakage and bursting pressures.

Exposure of the tissue to the NIR laser for 5 and 7 min resulted in similar tissue leaking/bursting pressures; however, tissue charring and shrinkage were observed after irradiation for 7 min. Overall, laser irradiation of nanocomposites (GNR 5.4 wt %) for 5 min provided optimal tissue welding and resulted in tissue leaking

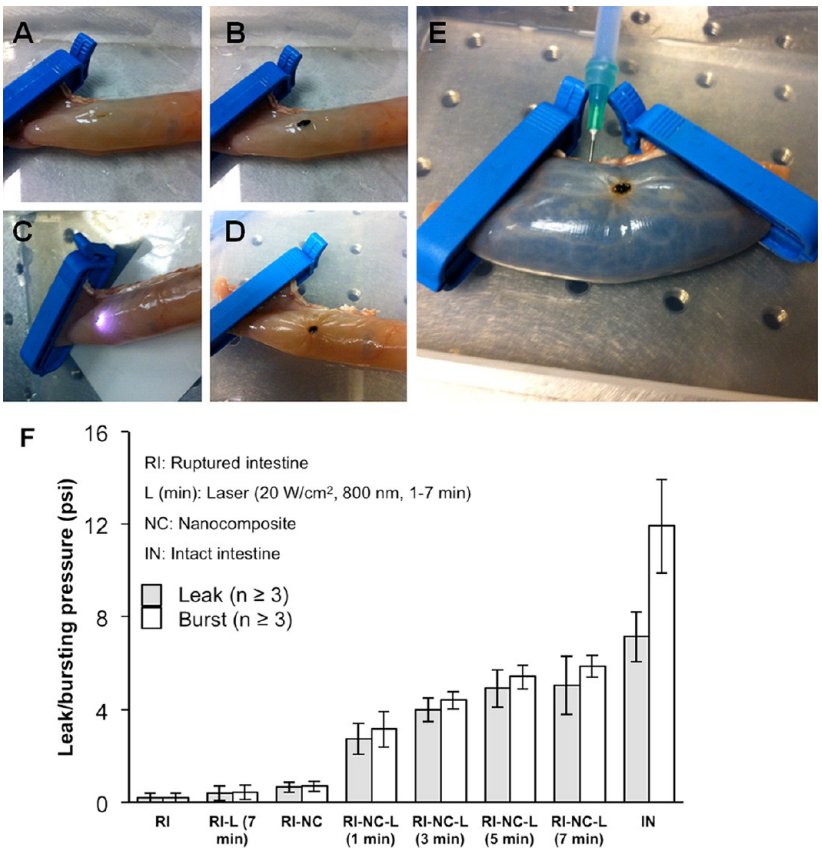

Figure 4. Bursting and leakage studies following laser tissue welding of intestines using nanocomposites. (A) A 5 mm incision was first applied to the intestine. (B) Nanocomposite (~2 mg) was then applied to the cut, and (C) irradiated with a laser at 20 W/cm^2, resulting in (D) a fluid-tight sealing. (E) The leaking and bursting pressures were measured and reported. (F) Bursting and leakage pressures of tissues before and after laser tissue welding using nanocomposite solders.

and bursting pressure recovery from 3% up to 71% and 45% of the their original intact forms, respectively.

Leakage of bacteria from intestinal tissue was investigated following incision closure using nanocomposite-assisted laser welding. On the basis of our previous optimization, we employed nanocomposites (~2 mg), at a fixed GNR concentration of 5.4 wt %, to weld a 5 mm incision located at the center of tubular porcine small intestine (~10 cm in length) using NIR laser irradiation (20 W/cm^2, 5 min). DH5-α *E. coli* cells were employed as model bacteria to mimic the inner condition of the intestine. Note that the bacterial concentration in intestine sections is 10^5-10^9 bacteria/gram of intestinal contents;[50,51] *E. coli* cell cultures with an OD_{600} of 0.5 are approximately 4×10^8 bacteria per mL. Leakage of DH5-α cells from inside the intestine to the surrounding fresh LB culture broth was followed as an indication of resistance to infection. The schematic of the experimental setup is shown in Figure 5A.

Rupture of the small intestine resulted in leakage of DH5-α cells into the fresh LB broth, leading to an increase in turbidity of the surrounding medium as measured using optical density at 600 nm, or OD_{600}. No leakage was observed in the case of the intact intestine (control, Figure 5B) and the ruptured intestine treated with the nanocomposite and NIR laser irradiation (Figure 5C) two hours after introducing DH5-α cells (10 mL, $OD_{600} = 0.5$) into the tubular small intestines. In these cases, the fresh LB broth remained clear or nonturbid. Conversely, in Figure 5D and E, the untreated ruptured intestine and ruptured intestine treated with laser alone (without nanocomposite) did not prevent leakage of bacteria; a significant increase in LB broth optical density was observed.

Figure 5F and G provide a quantitative analysis of the bacterial leakage, based on OD_{600}. Bacterial leakage was immediately observed upon introduction of DH5-α cells into the tubular intestines in the case of untreated ruptured intestine, ruptured intestine treated with the NIR laser alone (no nanocomposite), and ruptured intestine treated with nanocomposite alone (no laser) conditions (Figure 5F, white markers). In all these cases, OD_{600} of the fresh LB broth increased from 0 at 0 h to 0.22 ± 0.03 at 4 h, indicating growth of leaked bacterial in the fresh LB broth medium. These initial increases in optical density of fresh LB broth were followed by a gradual decrease in OD_{600} from 0.22 ± 0.03 to 0.09 ± 0.03 between 4 and 8 h, which is likely due to the stationary and autolytic phases of DH5-α cells.[52,53] Finally, a steady increase in OD_{600} from 0.09 ± 0.03 up

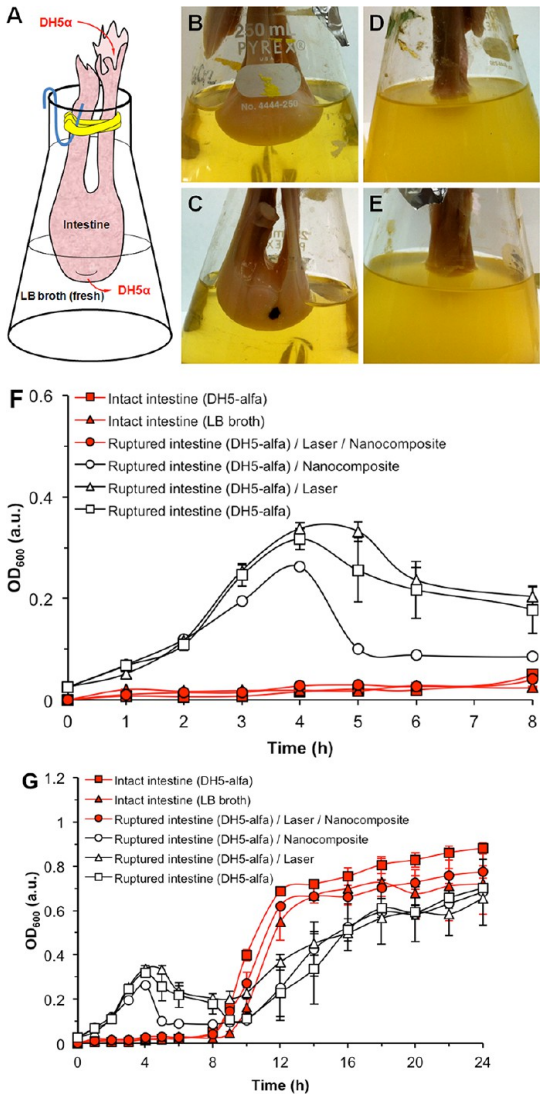

Figure 5. (A) Schematic depicting the experimental setup for the bacterial leakage study. At 2 h after introduction of DH5-α cells, no leakage was observed in the case of (B) intact intestine control and (C) nanocomposite-assisted, laser-welded ruptured intestine. The fresh LB broth remained clear and uncontaminated. (D) Ruptured intestine and (E) laser-treated (without nanocomposite) ruptured intestine did not provide a liquid-tight sealing, which resulted in bacterial leakage and growth in fresh LB broth medium. (F and G) Change in OD_{600} of fresh LB broth was monitored as a function of time (E: 0−8 h, F: 0−24 h) and at different treatment conditions for quantitative comparison.

0.66 ± 0.16 was observed between 8 and 24 h (Figure 5G, white markers). This reflects the growth of pre-existing bacteria in the intestinal tissues.

For the condition where ruptured intestine was welded with both nanocomposite and NIR laser (Figure 5F, red circle markers), the optical density (OD_{600}) of the fresh LB broth remained low at 0.04 ± 0.007 up to 8 h after introduction of DH5-α cells into the tubular intestine, indicating no DH5-α leakage. An increase in optical density (up to 0.72 ± 0.25) at 600 nm was observed after 8 h (Figure 5G, red circle markers). Both controls, intact intestine filled with either DH5-α cells or fresh LB broth without bacteria (Figure 5G, red square and triangle markers), showed a growth in turbidity similar to the nanocomposite-assisted, laser-welded ruptured intestine samples (Figure 5G, red circle markers), confirming that bacterial growth between 8 and 24 h is due to pre-existing bacteria in the tissue and not from the leakage of DH5-α cells into fresh LB broth medium. In addition, the overall growth of bacteria in conditions associated with DH5-α leakage (Figure 5G, white markers) is less pronounced than those without DH5-α leakage (Figure 5G, red markers). This is presumably due to the depletion of nutrients and the growth competition between DH5-α and intestinal bacteria associated with the tissues. Overall, ruptured intestines that underwent laser tissue welding using nanocomposites can provide a fluid-tight sealing and prevent bacterial leakage. The leakage prevention was successful, and we observed that the laser-activated nanocomposite continued to provide a liquid-tight sealing for at least one week, which was the duration of these studies (not shown).

The above studies indicate strong translational potential of the plasmonic nanocomposites in clinical applications, although detailed studies will be needed as part of future work. In all these studies, laser tissue welding was carried out using a laser power density of 20 W/cm^2, which is similar to that employed in other *in vitro* and *in vivo* studies.[13,22,54] Laser energies employed in preclinical laser tissue welding typically range from 3 to 20 J/mm,[13,22,54] while clinical laser-assisted scar healing employs approximately 0.5 J/mm to reduce charring.[55] In our study, approximately 20 J/mm was employed for intestinal laser tissue welding, which is within the limit of preclinical studies. It is important to note that clinical translation of laser welding with the current nanocomposites will require further optimization of laser dosage and nanoparticle:polypeptide ratios under the guidance of real-time photothermal response monitoring and predictive mathematical modeling *in vivo* in order to prevent undesired peripheral tissue damage. Although better than visible light, penetration of near-infrared light is restricted *in vivo*, which can be limiting for laser-based welding of different tissues. However, it is anticipated that these materials will be used for anastomosis after removal of diseased tissue during surgery, when the tissue is opened and accessible to laser light. We chose ELPs and GNRs in the current study, since both materials have been demonstrated to be biocompatible in preclinical studies. ELPs have been shown to degrade over time; degradation rates of 4%/day and 2.5 wt %/day were reported in fresh mouse serum[56] and in nude mice,[57] respectively. The long-term residence/clearance of gold nanorods *in vivo* has not been entirely elucidated, but gold nanoshells (Auroshell), under investigation for hyperthermia treatment of head and neck cancer disease, showed negligible toxicity in beagle dogs after 10 months.[58] Taken

together, these plasmonic nanocomposites are exciting materials for laser-based tissue repair.

CONCLUSIONS

In this study, we investigated biocompatible gold nanorod–elastin-like polypeptide nanocomposites as plasmonic biomaterial "solders" for intestinal tissue repair using NIR laser-based tissue welding. Engineered cysteine-containing ELPs (C_{12}ELPs) were selected mainly due to their elasticity, thermal response, stability, and biocompatibility. Gold nanorods were employed with the dual purpose of cross-linking ELPs, leading to a stabilized matrix with tunable stiffness, and for their plasmonic/photothermal properties. Both cellular and acellular GNR–C_{12}ELP nanocomposites were able to successfully repair ruptured intestinal tissue upon laser irradiation, with minimal tissue charring and shrinkage. Significant enhancements in recovery of leakage and bursting pressures, as well as tensile strength of the repaired intestines, were observed. Laser welding using the plasmonic nanocomposites also resulted in prevention of bacterial leakage from the intestine to the surroundings, indicating their potential in reducing anastomotic leakage. These nanocomposites possess tremendous translational potential in the repair of intestinal and colorectal tissues in several diseases, including cancer. Use of therapeutically relevant cells, including stem cells, and encapsulation of drugs within the nanocomposite can further enhance healing and repair, while preventing infection. Future work will involve optimization of parameters employed in laser-based tissue welding using these nanocomposites, comparison with traditional dyes, spatiotemporal mapping of photothermal responses, and photothermally triggered release of therapeutic molecules, leading to preclinical evaluation of these promising materials.

EXPERIMENTAL SECTION

Materials. Gold(III) chloride trihydrate ($HAuCl_4 \cdot 3H_2O$), cetyltrimethyl ammonium bromide (CTAB), L-ascorbic acid, sodium borohydride, and silver nitrate were purchased from Sigma-Aldrich. Reductacryl resin was purchased from EMD. All chemicals were used as received without further purification. DMEM cell culture medium was purchased from Invitrogen. Pen-Strep solution (10 000 units/mL penicillin and 10 000 μg/mL streptomycin in 0.85% NaCl) and fetal bovine serum (FBS) were purchased from Hyclone. Fresh porcine small intestines were purchased from Animal Technologies Inc., Texas. Luria–Bertani (LB) broth was purchased from Fisher Scientific.

Gold Nanorod Synthesis and Characterization. The seed-growth method[59] was employed for the generation of gold nanorods. All chemicals were freshly prepared in nanopure water (resistivity, 18.2 MΩ-cm) for synthesis procedures. Briefly, a seed solution was prepared by sodium borohydride (0.6 mL, 0.01 M, 4 °C)-mediated reduction of $HAuCl_4 \cdot 3H_2O$ (5 mL, 0.5 mM) in CTAB (5 mL, 200 mM) under vigorous stirring. The growth solution was prepared by adding L-ascorbic acid (280 μL, 0.0788 M) to reduce $HAuCl_4 \cdot 3H_2O$ (20 mL, 0.001 M) in CTAB solution (20 mL, 200 mM) containing silver nitrate (1080 μL, 0.004 M). The seed solution (50 μL) was introduced to a 40 mL growth solution overnight under continuous stirring at 28 °C, which resulted in the formation of gold nanorods stabilized by a CTAB bilayer.[60] These GNRs possessed absorbance maxima (λ_{max}) in the near-infrared region (700–1000 nm) of the light absorption spectrum. Nanorod aliquots, with an initial CTAB concentration of 100 mM, were pelleted by centrifugation (6000 rcf, 10 min), following which the clear supernatant was removed and resuspended in nanopure water to various final volumes. Further centrifugation, decantation, and dilution steps allowed the generation of a series of nanorod samples (9.5–190 μg/mL) with CTAB concentration less than 0.25 mM; we have previously determined that this CTAB concentration is optimal for nanocomposite formation.[61] In all cases, the concentration of gold in GNRs was determined using inductively coupled plasma optical emission spectrometry (ICP-OES, iCAP 6000 Series, Thermo Electron Corporation); NIR light absorption characteristics of the nanorods were determined using a plate reader (Biotek Synergy 2).

Preparation of Poly(ethylene glycol)-Modified Gold Nanorods. Aliquots of gold nanorod dispersions (19 μg/mL) were centrifuged at 6000 rcf for 10 min. The supernatants were decanted, and the GNR precipitates were resuspended in mPEG5000-SH solutions (Creative PEGWorks) at various concentrations (50–250 μg/mL) for 2 h at room temperature. Free mPEG5000-SH molecules were removed by centrifugation at 6000 rcf for 10 min.[62] The final PEG–GNRs were resuspended in nanopure water.

Synthesis, Expression, and Purification of Elastin-like Polypeptides. Elastin-like polypeptides, containing 12 cysteines residues (C_{12}ELP) in the repetitive sequence, MVSACRGPG-(VG VPGVGVPGVGVPGVGVPGVGVPG)$_8$-(VG VPGVG VPGVG VPGCG VPGVG VPG)$_{12}$-WP, were generated *via* recursive directional ligation.[63] The C_{12} in the C_{12}ELP name indicates the presence of 12 cysteines in the ELP repeat sequence. Oligonucleotides encoding ELPs were first cloned into pUC19, followed by cloning into a modified version of the pET25b+ expression vector at the sfil site. *Escherichia coli* BLR(DE3) (Novagen) was used as a bacterial host for polypeptide expression, followed by purification, lyophilization, and storage at 4 °C as described previously.

Preparation of GNR–C_{12}ELP Nanocomposite. Preparation of GNR–C_{12}ELP nanocomposites follows two distinct steps as described previously:[61,64] (i) self-assembly of C_{12}ELPs on GNRs *via* gold–thiol bonds at 4 °C leading to the formation of GNR–C_{12}ELP dispersions (nanoassemblies) and (ii) phase separation (coacervation and maturation) of these nanoassemblies, leading to the irreversible formation of solid-phase nanocomposites at 37 °C. GNRs (9.5–190 μg/mL in nanopure water) at a volume of 1 mL were mixed with 1 mL of C_{12}ELP (2 mg/mL, 1 × PBS) overnight at 4 °C. This led to the formation of GNR–C_{12}ELP nanoassemblies with various GNR weight percentages (0.47–8.7 wt %). GNR–C_{12}ELP nanoassemblies (2 mL) were placed in a homemade device and incubated at 37 °C for 6 h, leading to the formation of GNR–C_{12}ELP nanocomposites (10 mm diameter, thickness = 247 ± 65 μm) on top of a glass coverslip. The thickness of the nanocomposites was determined using a digital caliper and light microscopy. Similar procedures were followed for preparing PEG–GNR–C_{12}ELP nanocomposites consisting of PEG-modified gold nanorods. The successful binding of C_{12}ELP to PEGylated gold nanorods was confirmed experimentally using a BCA protein assay kit (Thermo Scientific). The binding percentage of C_{12}ELP to PEG-modified nanorods is 78.4 ± 1.4 (%) (n = 6). In addition, 93.2 ± 2.2 (%) (n = 6) of the PEG–GNR–C_{12}ELP nanoassemblies phase separated into solid nanocomposite upon temperature elevation.

Swelling Studies. GNR–C_{12}ELP nanocomposite samples were incubated in 2 mL of 1 × PBS (pH 7.4) at 25 °C for 24 h, following which the mass of the nanocomposite plus the tube was measured. The mass of the swollen nanocomposite (M_s) was determined by subtracting the mass of the tube from the total mass. The nanocomposites were freeze-dried using lyophilizer

(FreeZone, Labconco Corporation). The dry mass (M_d) was calculated by subtracting the mass of the tube from the total mass. The swelling ratio (Q) is defined as the weight fractional increase of the nanocomposite due to water absorption, where $Q = (M_s - M_d)/M_d$.[65]

Rheological Measurements. Mechanical properties of GNR−C_{12}ELP nanocomposites and C_{12}ELP coacervates were assessed using an AR-G2 rheometer (TA Instruments) in a parallel plate configuration (8 mm diameter). The samples (10 mm diameter, ~1 mm thickness) were loaded between the plates, and the gap was closed until the sample was in good contact with both plates (normal force <0.1 N). Prior to measurement, samples were equilibrated on a temperature-controlled Peltier plate for 30 min in order to exclude the time-dependent relaxation during the measurement. The dynamic frequency sweep was conducted over an angular frequency range of 1−40 rad/s, at a fixed strain amplitude of 0.05 and 25 °C. A temperature sweep was performed between 25 and 45 °C at a temperature increment rate of 1 °C/min, and the frequency and strain amplitude were controlled at 20 rad/s and 0.05, respectively. The absolute shear modulus ($|G^*|$) and tangent of the loss angle (tan δ), representing the stiffness and the relative measure of viscous to elastic effects of the nanocomposite under dynamic loading, respectively, were calculated. The absolute magnitude of the shear modulus, $|G^*|$, was determined based on the definition $|G^*| = (G'^2 + G''^2)^{0.5}$, where G' and G'' are the elastic storage modulus and the viscous loss modulus, respectively. The tangent of the loss angle was determined based on ($\tan \delta = G''/G'$). Note that for purely elastic ideal solids the loss angle (δ) is 0°, while purely viscous Newtonian fluids have a loss angle (δ) equal to 90°.

Cell Culture on Nanocomposite Solders. NIH 3T3 murine fibroblast cells were cultured at 5% CO_2 and 37 °C using DMEM medium containing 10% heat-inactivated fetal bovine serum and 1% antibiotics. The biocompatibility of nanocomposites containing various GNR (1.9−5.4 wt %) and PEG (0−19.7 wt %) weight percentages was evaluated in 96-well plates. Nanocomposites were formed at the bottom of the wells and treated with serum-containing cell culture medium. Fibroblasts (5000 cells/well) were seeded on top of nanocomposites for 24, 48, and 72 h. Cell viability analyses were carried out using the fluorescence-based live/dead assay (Invitrogen) and a Zeiss AxioObserver D1 inverted microscope (Carl Zeiss MicroImaging Inc.). Quantitative analysis was carried out by counting cells using the ImageJ software.[61]

Laser Tissue Welding. A titanium sapphire laser pumped by a solid-state laser (Spectra-Physics, Millennia) was employed for laser tissue welding. The excitation source (continuous wave, 2 mm beam diameter) was tuned to overlap with the λ_{max} of the nanocomposites at 800 nm. Tissue samples were defrosted in nanopure water and kept moist at 25 °C for laser tissue welding.

Tensile Strength Measurements. An 8 mm full thickness incision was applied at the center of the intestine section (4 × 1 cm, ~0.1 cm thick). The incision edges were brought into contact with one another, and nanocomposite (1 cm diameter) was applied on top of the serosa layer and across the incision with full contact (Figure 3A). Laser irradiation (20 W/cm^2) was applied vertically at a speed of 1 mm/s across the nanocomposite for 60 s, and samples were kept moist during welding to minimize charring. After welding, tissue tensile strength was measured using a TA XT Plus texture analyzer (Texture Technology Corp., NY) with a 5 kg load cell. Welded tissues were held with pneumatic grips to prevent slipping during testing. Testing was carried out in the tension mode at a rate of 0.5 mm/s until failure. The maximum force (N) achieved before tissue breakage was recorded and reported as ultimate tensile strength (UTS, kPa). Intact porcine small intestine sections were subjected to mechanical testing to determine the UTS of uncut specimens. Data reported represent the mean ± one standard deviation from at least three and up to 12 individual samples.

Leakage and Bursting Pressure Measurement. Bursting and leaking pressure tests were conducted on tubular porcine intestines. A homemade pressure detection system was designed and built (Figure S4). The tubular porcine intestines were cut into approximately 10 cm sections, leaving both ends opened. A full thickness incision (~5 mm) was applied to the center of the tubular intestine. The nanocomposite was applied to the incision. The CW laser (20 W/cm^2) was then applied to the nanocomposite (GNR 5.4 wt %) and tissue for various durations (1, 3, 5, and 7 min). After LTW was complete, the intestines were tightly clamped at both ends. A 21G1 Precision Glide needle was inserted into the tissue, and dyed water was fed into the intestine sections. The pressure was monitored and recorded at the leaking and bursting points. The leaking pressure was defined as when the first drop of colored water was seen coming out of the weld site.[65] The bursting pressure was defined as when a stream of water was seen coming out of the weld site. Control bursting and leaking pressure tests were conducted on intact and cut tissues. The bursting pressure site was always along the length of the intestine. Dye leakage from the needle puncture site was considered negligible.

Bacteria Leakage Study. The leakage of *E. coli* DH5-α bacterial cells from intestines was evaluated. A 5 mm incision was applied to the center of each 10 cm tubular intestine and subjected to different treatments (Figure 5A). Immediately after treatment, the tubular intestines were hung vertically in Erlenmeyer flasks (each filled with 190 mL of fresh LB broth), leaving the two open ends pointing up. The U-shape hanging method ensures the incision (or welded) sites were submerged in the fresh LB broth. A 10 mL culture of bacterial cells at an optical density (OD_{600}) of 0.5 was placed inside the intestine and allowed to incubate (37 °C, 100 rpm). The optical densities of the fresh LB broth were monitored as a function of time as an indication for leakage.

Conflict of Interest: The authors declare no competing financial interest.

Acknowledgment. The authors thank Professor Lenore L. Dai, Chemical Engineering, Arizona State University (ASU), Tempe, AZ, for access to the rheometer and texture analyzer. The authors also acknowledge Dr. Su Lin for access to the Ultrafast laser facility at ASU. We thank Dr. Christine Pauken, Biomedical Engineering, ASU, and Professor Michael Sierks, Chemical Engineering, ASU, for NIH 3T3 and DH5-α *E. coli* cells, respectively. The authors also thank Mr. Fred Peña and Mr. Caesario Sutiyoso, an undergraduate student at ASU, for excellent technical assistance. This work was supported by the Defense Threat Reduction Agency Young Investigator Award (HDTRA1-10-1-0109) to K.R. and a Fulton Undergraduate Research Initiative (FURI) Award at ASU to A.N.

Supporting Information Available: This material is available free of charge *via* the Internet at http://pubs.acs.org.

REFERENCES AND NOTES

1. Hyman, N.; Manchester, T. L.; Osler, T.; Burns, B.; Cataldo, P. A. Anastomotic Leaks after Intestinal Anastomosis - It's Later than You Think. *Ann. Surg.* **2007**, *245*, 254–258.
2. Karanjia, N. D.; Corder, A. P.; Bearn, P.; Heald, R. J. Leakage from Stapled Low Anastomosis after Total Mesorectal Excision for Carcinoma of the Rectum. *Brit. J. Surg.* **1994**, *81*, 1224–1226.
3. Isbister, W. H. Anastomotic Leak in Colorectal Surgery: A Single Surgeon's Experience. *Anz. J. Surg.* **2001**, *71*, 516–520.
4. Park, I. J. Influence of Anastomotic Leakage on Oncological Outcome in Patients with Rectal Cancer. *J. Gastrointest. Surg.* **2010**, *14*, 1190–1196.
5. Catena, F.; La Donna, M.; Gagliardi, S.; Avanzolini, A.; Taffurelli, M. Stapled *versus* Hand-Sewn Anastomoses in Emergency Intestinal Surgery: Results of a Prospective Randomized Study. *Surg. Today* **2004**, *34*, 123–126.
6. Thomson, G. A. An Investigation of Leakage Tracts along Stressed Suture Lines in Phantom Tissue. *Med. Eng. Phys.* **2007**, *29*, 1030–1034.
7. Zuger, B. J.; Ott, B.; Mainil-Varlet, P.; Schaffner, T.; Clemence, J. F.; Weber, H. P.; Frenz, M. Laser Solder Welding of Articular Cartilage: Tensile Strength and Chondrocyte Viability. *Laser Surg. Med.* **2001**, *28*, 427–434.
8. Wolf -de Jonge, I. C. D.; Beek, J. F.; Balm, R. 25 Years of Laser Assisted Vascular Anastomosis (LAVA): What Have We Learned? *Eur. J. Vasc. Endovasc.* **2004**, *27*, 466–476.

9. Matteini, P.; Rossi, F.; Menabuoni, L.; Pini, R. Microscopic Characterization of Collagen Modifications Induced by Low-temperature Diode-Laser Welding of Corneal Tissue. *Laser Surg. Med.* **2007**, *39*, 597–604.
10. Wadia, Y.; Xie, H.; Kajitani, M. Liver Repair and Hemorrhage Control by Using Laser Soldering of Liquid Albumin in a Porcine Model. *Laser Surg. Med.* **2000**, *27*, 319–328.
11. Kirsch, A. J.; Miller, M. I.; Hensle, T. W.; Chang, D. T.; Shabsigh, R.; Olsson, C. A.; Connor, J. P. Laser-Tissue Soldering in Urinary-Tract Reconstruction - First Human-Experience. *Urology* **1995**, *46*, 261–266.
12. Schober, R.; Ulrich, F.; Sander, T.; Durselen, H.; Hessel, S. Laser-Induced Alteration of Collagen Substructure Allows Microsurgical Tissue Welding. *Science* **1986**, *232*, 1421–1422.
13. Gobin, A. M.; O'Neal, D. P.; Watkins, D. M.; Halas, N. J.; Drezek, R. A.; West, J. L. Near Infrared Laser-Tissue Welding Using Nanoshells as an Exogenous Absorber. *Laser Surg. Med.* **2005**, *37*, 123–129.
14. Yang, P.; Yao, M.; DeMartelaere, S. L.; Redmond, R. W.; Kochevar, I. E. Light-Activated Sutureless Closure of Wounds in Thin Skin. *Laser Surg. Med.* **2011**, *44*, 163–167.
15. Matteini, P.; Ratto, F.; Rossi, F.; Cicchi, R.; Stringari, C.; Kapsokalyvas, D.; Pavone, F. S.; Pini, R. Photothermally-Induced Disordered Patterns of Corneal Collagen Revealed by SHG Imaging. *Opt. Express.* **2009**, *17*, 4868–4878.
16. Bass, L. S.; Moazami, N.; Pocsidio, J.; Oz, M. C.; Logerfo, P.; Treat, M. R. Changes in Type-I Collagen Following Laser-Welding. *Laser Surg. Med.* **1992**, *12*, 500–505.
17. Murray, L. W.; Su, L.; Kopchok, G. E.; White, R. A. Crosslinking of Extracellular-Matrix Proteins - a Preliminary-Report on a Possible Mechanism of Argon-Laser Welding. *Laser Surg. Med.* **1989**, *9*, 490–496.
18. Cilesiz, I.; Springer, T.; Thomsen, S.; Welch, A. J. Controlled Temperature Tissue Fusion: Argon Laser Welding of Canine Intestine *in Vitro*. *Laser Surg. Med.* **1996**, *18*, 325–334.
19. Chikamatsu, E.; Sakurai, T.; Nishikimi, N.; Yano, T.; Nimura, Y. Comparison of Laser Vascular Welding, Interrupted Sutures, and Continuous Sutures in Growing Vascular Anastomoses. *Laser Surg. Med.* **1995**, *16*, 34–40.
20. Gennaro, M.; Ascer, E.; Mohan, C.; Wang, S. A Comparison of CO_2 Laser-Assisted Venous Anastomoses and Conventional Suture Techniques - Patency, Aneurysm Formation, and Histologic Differences. *J. Vasc. Surg.* **1991**, *14*, 605–613.
21. Grubbs, P. E.; Wang, S.; Marini, C.; Basu, S.; Rose, D. M.; Cunningham, J. N. Enhancement of CO_2-Laser Microvascular Anastomoses by Fibrin Glue. *J Surg. Res.* **1988**, *45*, 112–119.
22. Matteini, P.; Ratto, F.; Rossi, F.; Rossi, G.; Esposito, G.; Puca, A.; Albanese, A.; Maira, G.; Pini, R. *In Vivo* Carotid Artery Closure by Laser Activation of Hyaluronan-Embedded Gold Nanorods. *J. Biomed. Opt.* **2010**, *15*, 0415081–0415086.
23. Matteini, P.; Ratto, F.; Rossi, F.; Centi, S.; Dei, L.; Pini, R. Chitosan Films Doped with Gold Nanorods as Laser-Activatable Hybrid Bioadhesives. *Adv. Mater.* **2010**, *22*, 4313–4316.
24. Huang, H. C.; Yang, Y.; Nanda, A.; Koria, P.; Rege, K. Synergistic Administration of Photothermal Therapy and Chemotherapy to Cancer Cells using Polypeptide-Based Degradable Plasmonic Matrices. *Nanomedicine* **2011**, *6*, 459–473.
25. Qin, Z. P.; Bischof, J. C. Thermophysical and Biological Responses of Gold Nanoparticle Laser Heating. *Chem. Soc. Rev.* **2012**, *41*, 1191–1217.
26. Huang, X. H.; Jain, P. K.; El-Sayed, I. H.; El-Sayed, M. A. Plasmonic Photothermal Therapy (PPTT) Using Gold Nanoparticles. *Lasers Med. Sci.* **2008**, *23*, 217–228.
27. Hirsch, L. R.; Gobin, A. M.; Lowery, A. R.; Tam, F.; Drezek, R. A.; Halas, N. J.; West, J. L. Metal Nanoshells. *Ann. Biomed. Eng.* **2006**, *34*, 15–22.
28. Mackay, J. A.; Chilkoti, A. Temperature Sensitive Peptides: Engineering Hyperthermia-Directed Therapeutics. *Int. J. Hyperther.* **2008**, *24*, 483–495.
29. Koria, P.; Yagi, H.; Kitagawa, Y.; Megeed, Z.; Nahmias, Y.; Sheridan, R.; Yarmush, M. L. Self-assembling Elastin-like Peptides Growth Factor Chimeric Nanoparticles for the Treatment of Chronic Wounds. *Proc. Natl. Acad. Sci. U.S.A.* **2011**, *108*, 1034–1039.
30. Simnick, A. J.; Lim, D. W.; Chow, D.; Chilkoti, A. Biomedical and Biotechnological Applications of Elastin-like Polypeptides. *Polym. Rev.* **2007**, *47*, 121–154.
31. MacEwan, S. R.; Chilkoti, A. Elastin-Like Polypeptides: Biomedical Applications of Tunable Biopolymers. *Biopolymers* **2010**, *94*, 60–77.
32. Urry, D. W. Physical Chemistry of Biological Free Energy Transduction As Demonstrated by Elastic Protein-Based Polymers. *J. Phys. Chem. B* **1997**, *101*, 11007–11028.
33. McHale, M. K.; Setton, L. A.; Chilkoti, A. Synthesis and *in Vitro* Evaluation of Enzymatically Cross-linked Elastin-like Polypeptide Gels for Cartilaginous Tissue Repair. *Tissue Eng.* **2005**, *11*, 1768–1779.
34. Betre, H.; Setton, L. A.; Meyer, D. E.; Chilkoti, A. Characterization of a Genetically Engineered Elastin-like Polypeptide for Cartilaginous Tissue Repair. *Biomacromolecules* **2002**, *3*, 910–916.
35. Trabbic-Carlson, K.; Setton, L. A.; Chilkoti, A. Swelling and Mechanical Behaviors of Chemically Cross-linked Hydrogels of Elastin-like Polypeptides. *Biomacromolecules* **2003**, *4*, 572–580.
36. Nettles, D. L.; Chilkoti, A.; Setton, L. A. Applications of Elastin-like Polypeptides in Tissue Engineering. *Adv. Drug Delivery Rev.* **2010**, *62*, 1479–1485.
37. Minato, A.; Ise, H.; Goto, M.; Akaike, T. Cardiac Differentiation of Embryonic Stem Cells by Substrate Immobilization of Insulin-like Growth Factor Binding Protein 4 with Elastin-like Polypeptides. *Biomaterials* **2012**, *33*, 515–523.
38. Mie, M.; Mizushima, Y.; Kobatake, E. Novel Extracellular Matrix for Cell Sheet Recovery Using Genetically Engineered Elastin-like Protein. *J. Biomed. Mater. Res., Part A* **2008**, *86B*, 283–290.
39. Bhattarai, N.; Edmondson, D.; Veiseh, O.; Matsen, F. A.; Zhang, M. Q. Electrospun Chitosan-Based Nanofibers and Their Cellular Compatibility. *Biomaterials* **2005**, *26*, 6176–6184.
40. Betre, H.; Ong, S. R.; Guilak, F.; Chilkoti, A.; Fermor, B.; Setton, L. A. Chondrocytic Differentiation of Human Adipose-Derived Adult Stem Cells in Elastin-like Polypeptide. *Biomaterials* **2006**, *27*, 91–99.
41. Poppas, D. P.; Stewart, R. B.; Massicotte, M.; Wolga, A. E.; Kung, R. T. V.; Retik, A. B.; Freeman, M. R. Temperature-Controlled Laser Photocoagulation of Soft Tissue: *In Vivo* Evaluation Using a Tissue Welding Model. *Laser Surg. Med.* **1996**, *18*, 335–344.
42. Wise, L.; McAlister, W.; Stein, T. Studies on the Healing of Anastomoses of Small and Large Intestines. *J. Surg. Gynecol. Obstet.* **1975**, *141*, 190−194.
43. Pasternak, B.; Rehn, M.; Andersen, L.; Agren, M. S.; Heegaard, A. M.; Tengvall, P.; Aspenberg, P. Doxycycline-Coated Sutures Improve Mechanical Strength of Intestinal Snastomoses. *Int. J. Colorectal Dis.* **2008**, *23*, 271–276.
44. Aumailley, M.; Krieg, T.; Razaka, G.; Muller, P. K.; Bricaud, H. Influence of Cell Density on Collagen Biosynthesis in Fibroblast Cultures. *Biochem. J.* **1982**, *206*, 505–10.
45. Ryoo, S. R.; Kim, Y. K.; Kim, M. H.; Min, D. H. Behaviors of NIH-3T3 Fibroblasts on Graphene/Carbon Nanotubes: Proliferation, Focal Adhesion, And Gene Transfection Studies. *ACS Nano* **2010**, *4*, 6587–6598.
46. Kim, H. N.; Hong, Y.; Kim, M. S.; Kim, S. M.; Suh, K. Y. Effect of Orientation and Density of Nanotopography in Dermal Wound Healing. *Biomaterials* **2012**, *33*, 8782–8792.
47. Lipska, M. A.; Bissett, I. P.; Parry, B. R.; Merrie, A. E. H. Anastomotic Leakage after Lower Gastrointestinal Anastomosis: Men Are at a Higher Risk. *Anz. J. Surg.* **2006**, *76*, 579–585.
48. Post, S.; Betzler, M.; Vonditfurth, B.; Schurmann, G.; Kuppers, P.; Herfarth, C. Risks of Intestinal Anastomoses in Crohns-Disease. *Ann Surg.* **1991**, *213*, 37–42.

49. Pickleman, J.; Watson, W.; Cunningham, J.; Fisher, S. G.; Gamelli, R. The Failed Gastrointestinal Anastomosis: An Inevitable Catastrophe? *J. Am. Coll. Surgeons* **1999**, *188*, 473–482.
50. Hooper, L. V.; Wong, M. H.; Thelin, A.; Hansson, L.; Falk, P. C.; Gordon, J. I. Molecular Analysis of Commensal Host-Microbial Relationships in the Intestine. *Science* **2001**, *291*, 881–884.
51. Husebye, E.; Hellstrom, P. M.; Sundler, F.; Chen, J.; Midtvedt, T. Influence of Microbial Species on Small Intestinal Myoelectric Activity and Transit in Germ-Free Rats. *Am. J. Physiol-Gastroenterol.* **2001**, *280*, G368–G380.
52. Leduc, M.; Kasra, R.; Vanheijenoort, J. Induction and Control of the Autolytic System of *Escherichia coli*. *J. Bacteriol.* **1982**, *152*, 26–34.
53. Leduc, M.; Vanheijenoort, J. Autolysis of *Escherichia coli*. *J. Bacteriol.* **1980**, *142*, 52–59.
54. Lauto, A.; Hook, J.; Doran, M.; Camacho, F.; Poole-Warren, L. A.; Avolio, A.; Foster, L. J. R. Chitosan Adhesive for Laser Tissue Repair: *In Vitro* Characterization. *Laser Surg. Med.* **2005**, *36*, 193–201.
55. Capon, A. C.; Gosse, A. R.; Iarmarcovai, G. N. K.; Cornil, A. H.; Mordon, S. R. Sear Prevention by Laser-Assisted Scar Healing (LASH): A Pilot Study Using an 810-nm Diode-Laser System. *Laser Surg. Med.* **2008**, *40*, 443–445.
56. Liu, W.; Dreher, M. R.; Chow, D. C.; Zalutsky, M. R.; Chilkoti, A. Tracking the in Vivo Fate of Recombinant Polypeptides by Isotopic Labeling. *J. Controlled Release* **2006**, *114*, 184–92.
57. Liu, W.; Dreher, M. R.; Furgeson, D. Y.; Peixoto, K. V.; Yuan, H.; Zalutsky, M. R.; Chilkoti, A. Tumor Accumulation, Degradation and Pharmacokinetics of Elastin-Like Polypeptides in Nude Mice. *J. Controlled Release* **2006**, *116*, 170–178.
58. Gad, S. C.; Sharp, K. L.; Montgomery, C.; Payne, J. D.; Goodrich, G. P. Evaluation of the Toxicity of Intravenous Delivery of Auroshell Particles (Gold-Silica Nanoshells). *Int. J. Toxicol.* **2012**, *31*, 584–594.
59. Nikoobakht, B.; El-Sayed, M. A. Preparation and Growth Mechanism of Gold Nanorods (NRs) Using Seed-Mediated Growth Method. *Chem. Mater.* **2003**, *15*, 1957–1962.
60. Nikoobakht, B.; El-Sayed, M. A. Evidence for Bilayer Assembly of Cationic Surfactants on the Surface of Gold Nanorods. *Langmuir* **2001**, *17*, 6368–6374.
61. Huang, H. C.; Nanda, A.; Rege, K. Investigation of Phase Separation Behavior and Formation of Plasmonic Nanocomposites from Polypeptide-Gold Nanorod Nanoassemblies. *Langmuir* **2012**, *28*, 6645–6655.
62. Dickerson, E. B.; Dreaden, E. C.; Huang, X. H.; El-Sayed, I. H.; Chu, H. H.; Pushpanketh, S.; McDonald, J. F.; El-Sayed, M. A. Gold Nanorod Assisted Near-Infrared Plasmonic Photothermal Therapy (PPTT) of Squamous Cell Carcinoma in Mice. *Cancer Lett* **2008**, *269*, 57–66.
63. Meyer, D. E.; Chilkoti, A. Genetically Encoded Synthesis of Protein-Based Polymers with Precisely Specified Molecular Weight and Sequence by Recursive Directional Ligation: Examples from the Elastin-like Polypeptide System. *Biomacromolecules* **2002**, *3*, 357–367.
64. Huang, H. C.; Koria, P.; Parker, S. M.; Selby, L.; Megeed, Z.; Rege, K. Optically Responsive Gold Nanorod-Polypeptide Assemblies. *Langmuir* **2008**, *24*, 14139–14144.
65. Park, H.; Guo, X.; Temenoff, J. S.; Tabata, Y.; Caplan, A. I.; Kasper, F. K.; Mikos, A. G. Effect of Swelling Ratio of Injectable Hydrogel Composites on Chondrogenic Differentiation of Encapsulated Rabbit Marrow Mesenchymal Stem Cells *in Vitro*. *Biomacromolecules* **2009**, *10*, 541–546.